Radio Science

RESEARCH ARTICLE
10.1029/2021RS007418

Key Points:

- Effects in the GNSS signal, in the ionosphere and in the magnetic field H component of the September 2017 X9.3 and X1.3 solar flares

Correspondence to:
E. R. de Paula,
eurico.paula@inpe.br

Citation:
de Paula, E. R., Martinon, A. R. F., Carrano, C., Moraes, A. O., Neri, J. A. C. F., Cecatto, J. R., et al. (2022). Solar flare and radio burst effects on GNSS signals and the ionosphere during September 2017. *Radio Science*, *57*, e2021RS007418. https://doi.org/10.1029/2021RS007418

Received 20 DEC 2021
Accepted 1 OCT 2022

Solar Flare and Radio Burst Effects on GNSS Signals and the Ionosphere During September 2017

Eurico R. de Paula[1], André R. F. Martinon[1], Charles Carrano[2], Alison O. Moraes[3], José A. C. F. Neri[1], José R. Cecatto[1], Mangalathayil A. Abdu[1], Acácio C. Neto[1], João F. G. Monico[4], Weverton da Costa Silva[4], Bruno C. Vani[5], Inez S. Batista[1], Odim Mendes[1], Jonas R. de Souza[1], and André L. A. Silva[6]

[1]INPE, São José dos Campos, Brazil, [2]ISR, Boston College, Boston, MA, USA, [3]IAE, São José dos Campos, Brazil, [4]CT/UNESP, Presidente Prudente, Brazil, [5]IFSP, São Paulo, Brazil, [6]ITA, São José dos Campos, Brazil

Abstract Strong solar flare events can occur even during the decay phase of the solar cycle. During these events concurrent increases in the X-ray and Enhanced UV (EUV) fluxes and solar radio bursts (SRBs) can be observed. The SRBs cover a large range of frequencies including the L band, giving rise to signal fades in the GNSS carrier-to-noise ratio and fluctuations in its amplitude and phase. The increases in the X-ray, UV, and EUV fluxes cause increase in the ionospheric D, E, and F region electron densities. The aim of this work is to analyze the effects in the GNSS signal, in the ionosphere and in the magnetic field H component of the X9.3 and X1.3 solar flares that occurred on 06 and 07 September 2017, respectively. Data from a network of six GNSS receivers, two magnetometers, and four Digisondes are used in the analysis. Fades of about 5 and 10 dB were observed in the signals of GNSS L1 and L2/L5 frequencies, respectively. Significant positioning errors, were observed for the strongest X9.3 flare. A sudden increase in Total Electron Content with the rates of 2.5–5.0 TECU/min was observed. An increase in the E layer density gave origin to an increase in the Equatorial Electrojet intensity, whose signatures were observed in the H component of two magnetometers. Another observed effect was the ionospheric D region density increase that caused disruption in the Digisonde signal. As a consequence of the described effects, GNSS receivers may fail to produce accurate navigation solution.

1. Introduction

The effects of solar flares on the ionosphere have been studied for a long time (Mitra, 1974) and they were named Sudden Ionospheric Disturbances (SID). Enhanced UV (EUV) and X radiation during these events gives origin to impulsive ionization enhancements in the D, E, and F ionospheric layers. Many effects in the equatorial ionosphere during an X7/2B class flare, that occurred on 09 of August 2011, was presented by Sripathi et al. (2013). Liu et al. (2006) and Nogueira et al. (2015) and many others have studied the Total Electron Content (TEC) variations during solar flares. Besides the impulsive enhancements in the X, UV, and EUV radiation, simultaneous solar radio bursts (SRBs) are frequently observed during solar flares. Klobuchar et al. (1999) pointed out that the SRB could have the potential to cause harmful effects in the Global Positioning System (GPS) signals. Cerruti et al. (2006) pointed out that the GPS radio signals were designed as right-hand circularly polarized (RHCP) system and only SRB with the same polarization can efficiently affect the receiver signals. Cerruti et al. (2008) analyzed the effect of intense December 2006 SRBs on GPS receivers. According to Carrano et al. (2009) the SRBs occur in a large frequency range and in the GNSS L bands a drastic carrier-to-noise ratio (C/No) reduction can be observed since the solar radio signal acts as elevated background noise which competes with the broadcast GNSS signals, causing a degradation in the GNSS availability and positioning accuracy. Since then, many researchers have analyzed these effects and the consequent deterioration in the GNSS tracking and positioning accuracy (Sreeja et al., 2013). Yue et al. (2018) presented a detailed study on the effect of SRB on GNSS signal. Y. Yasyukevich et al. (2018) discussed the impact of the 06 September 2017 X-class solar flares on the GNSS, and HF radio wave propagation in the ionosphere. Curto et al. (2018) analyzed the effect of the solar flare of 06 September 2017 in the ionosphere as well as in the Earth's magnetic field. Tsurutani et al. (2009) described briefly the solar flare effects on the ionosphere. Hajra et al. (2020) provided a complete description of the space weather events during the September 2017 storm. Sato et al. (2019) studied the effects of the 06 September 2017 radio burst/EUV flare on GNSS signal and on positioning over Neustrelitz (53.32°N, 13.07°E), Germany longitudinal sector and using data from two other sites covering high [Ramfjordmoen (69.58°N, 19.23°E), Norway] and low latitude regions [Bahir Dar (11.57°N, 37.38°E), Ethiopia]. Recently Y. V. Yasyukevich et al. (2021) studied

Table 1
Strongest X Class Solar Flares Characteristics on 06 and 07 September 2017

Region	Class	Start (UT)	Maximum (UT)	End (UT)	Day
2673	X2.2	08:57	09:10	09:17	06 September 2017
2673	X9.3	11:53	12:02	12:10	06 September 2017
2674	X1.3	14:20	14:36	14:55	07 September 2017

the performance of the new GPS signals generated by the new GPS satellites IIR-M, GPS IIF and GPS III during solar flares that were accompanied by intense SRB.

Multiple space weather effects observed during two X class solar flares of 06 and 07 September 2017 are explored using multi-constellation daylight GNSS data from six receivers, four Digisondes, and two magnetometers. This multi-instrument study provides comparable results as the studies identified above with a new emphasis of these effects observed in the low latitude ionosphere in the Brazilian sector. The positioning errors during these events, using the RTKlib software, are also presented.

Solar parameters like EUV and X-ray fluxes and radio flux densities for these two events were plotted simultaneously with the GNSS data. 06–10 September 2017 was a geomagnetic disturbed period, when Sym-H magnetic index reached a minimum value of −146 nT on day 08 (de Paula et al., 2019) and in this period there occurred a series of solar flares. The characteristics of three of those flares are described in the next section. Physical mechanisms responsible for the flare effects in the ionosphere and in the magnetic field H component (Abdu et al., 2017) will be discussed.

2. Class X Events During 06 and 07 September 2017

Table 1 shows the strongest X class solar flares characteristics on 06 and 07 September 2017, according to website ftp.swpc.noaa.gov/pub/warehouse/2017/2017_events.tar.gz.

In this work we analyze the effects of the flare classes X9.3 and X1.3, when larger modifications on the GNSS signal, ionosphere and magnetic field H component were observed.

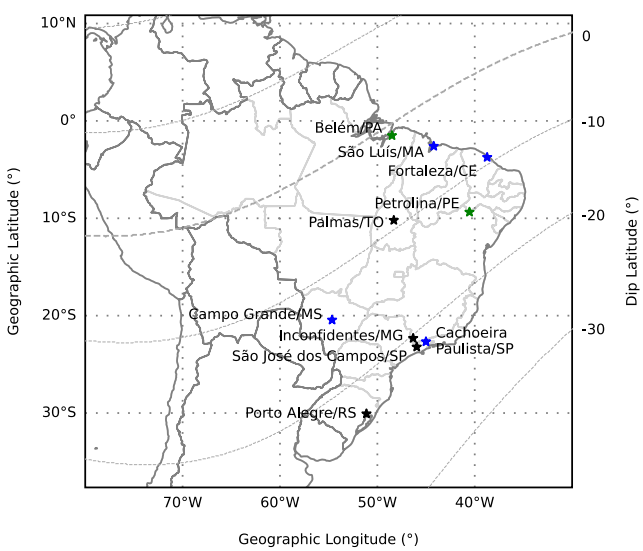

Figure 1. Map showing the São Luís, Fortaleza, Campo Grande, and Cachoeira Paulista Digisondes (blue stars), magnetometer (green stars) of Belém and Petrolina and GNSS Septentrio POLARxS PRO receiver sites (black stars). The GNSS sites are São Luís (blue star since it has also a Digisonde), Fortaleza, (blue star since it has also a Digisonde), Palmas, Inconfidentes, São José dos Campos, and Porto Alegre.

3. GNSS Receiver, Digisonde, Magnetometer, and Solar Radiation Data

Multi-constellation GNSS daylight data for the frequencies L1, L2C, and L5 over the Brazilian longitudinal sector (see Figure 1), measured by PolaRxS PRO Septentrio receivers using the Polant—MC AT1675-382 SW antenna, were analyzed during the X9.3 and X1.3 solar flare events on 06 and 07 September 2017, respectively. The GNSS C/No ratio was analyzed and the raw 50 Hz wideband signal intensity was used to infer the signal amplitude fluctuations. These fluctuations were quantified by the S4 index calculated as the signal intensity standard deviation relative to the average signal intensity for each 1 minute interval (de Paula et al., 2021). We deliberately named them amplitude fluctuations since they originated from the flares during daylight and their generation mechanisms are different from those of the post-sunset amplitude scintillation due to ionospheric irregularities generated over the magnetic dip equator. Additionally, the relative slant TEC (STEC) is calculated using the GNSS carrier phase data at a rate of one sample per 30 s from Rede Brasileira de Monitoramento Contínuo/Instituto Brasileiro de Geografia e Estatística (RMBC/IBGE) for the days 05–09 and over the site of São José dos Campos (23.18°S, 45.89°W, dip lat 21.22°S). The day 05 is magnetically quiet. Using these RBMC/IBGE data the Rate of TEC (ROT) and the Rate of TEC Index (ROTI) (Pi et al., 1997) were also calculated for this site and for days 05–07. The latitudinal variation of ROTI during the X9.3 event is also presented.

The solar flare effects on the H component of the magnetic field variations as recorded by the magnetometers located at Belém (1.5°S, 48.5°W, dip lat 1.12°S) and at Petrolina (09.4°S, 40.5°W, dip lat 13.45°S) and on the f_{min}

Table 2
Geographic Latitude, Longitude, and Dip Latitude of GNSS Receiver, Magnetometer, and Digisonde Sites

Site	Geographic latitude	Geographic longitude	Dip latitude
Belém[a]	01.45°S	48.50°W	01.12°S
São Luís (SLMA[b] and SAA0K[c])	02.53°S	44.31°W	04.67°S
Fortaleza (FRTZ[b] and FZA0M[c])	03.72°S	38.54°W	09.43°S
Petrolina[a]	09.39°S	40.51°W	13.45°S
Palmas (PALM[b])	10.17°S	48.33°W	09.17°S
Campo Grande (CGK21[c])	20.44°S	54.65°W	14.10°S
Inconfidentes (INCO[b])	22.32°S	46.33°W	20.33°S
Cachoeira Paulista (CAJ2M[c])	22.67°S	45.01°W	21.40°S
São José dos Campos (SJCU[b])	23.18°S	45.89°W	21.22°S
Porto Alegre (POAL[b])	30.03°S	51.23°W	23.37°S

[a]Magnetometer. [b]GNSS receiver. [c]Digisonde.

parameter registered by the Digisondes of São Luís (02.53°S, 44.31°W, dip lat 04.67°S), Fortaleza (03.72°S, 38.54°W, dip latitude 09.43°S), Campo Grande (20.44°S, 54.65°W, dip latitude 14.10°S), and Cachoeira Paulista (22.67°S, 45.01°W, dip latitude 21.40°S) were analyzed.

The soft and hard X-ray fluxes XRSA and XRSB respectively were obtained from the GOES satellite (https://satdat.ngdc.noaa.gov/sem/goes/data/science/xrs/goes15/gxrs-l2-irrad_science/2017/09/). The EUV data were available from the University of Colorado site (http://lasp.colorado.edu/eve/data_access/evewebdata/products/). The dynamic solar spectra were provided by the SWISS-BLEN5M data gathered from the e-Callisto International Network of Solar Radio Spectrometers. The BLEN5M radio flux is the sum of the RHCP and Left Hand Circular Polarization. Data from the Owens Valley Solar Array were not available for frequencies less than 3 GHz during this epoch.

Figure 1 shows the locations of the GNSS receivers, the Digisondes of São Luís, Fortaleza, Campo Grande, and Cachoeira Paulista and the magnetometers. The dip equator is shown as a thick dashed line, and dip latitudes at 10° intervals are marked as thin dashed lines.

Table 2 provides the geographic locations and the dip latitudes of these sites.

4. X9.3 and X1.3 Solar Flare Effects on the GNSS Signal and on the Slant TEC (STEC), Digisonde, and Magnetometer Data

4.1. GPS Signal Fades and Amplitude Fluctuations During the X9.3 and X1.3 Events

Figure 2 (upper panel) shows the soft (<100 KeV) and hard (10–200 KeV) GOES X-ray sensor fluxes XRSA (blue) and XRSB (orange) respectively, for 06 September 2017. The blue shaded region represents the occurrence time interval of the X9.3 event and the blue vertical continuous line is the time of the maximum intensity of this event (see Table 1). The EUV, X-ray and radio density fluxes remain elevated above their pre-event values beyond this time interval. Figure 2 (middle panel) presents the SWISS-BLEN5M solar radio flux density for the frequency range of 1,045–1,435 MHz. The solar radio flux density relative intensity for the frequency of 1,436.19 MHz (closer to the L1 frequency that was available from SWISS-BLEN5M for this date), for the frequency range 1,205.75–1,246.88 MHz that encompass the L2C frequency (1,227.60 MHz) and for the frequency range 1,155.69–1,197.00 MHZ that encompass the L5 frequency (1,176.60 MHZ) are presented in Figure 2 (lower panels) from left to right respectively. It is worth mentioning that similar recording was reported by Sato et al. (2019) where they show a sudden increase in the same time frame for observations made in San Vito. Figure 3 shows the GPS C/No signal for L1, L2C, and L5 GPS frequencies. Figure 4 shows the corresponding signal amplitude fluctuations represented by the S4 parameter for all visible PRNs as received at the sites FRTZ, INCO, and SJCU. No reliable data for L1 frequency for this date was available from INCO. The red dashed vertical lines mark the maximum intensity of the X9.3 flare.

Large C/No fades and S4 peaks reaching about 0.40 were observed in the L2C and L5 bands simultaneously with the solar flux density relative intensity increases centered around 12:02 and 12:08 UT. No C/No fades and amplitude fluctuations (S4) for the L1 band were detected on FRTZ and SJCU sites and INCO data were unreliable.

Figures 5–7 present the same parameters as those of Figures 2–4 for 07 September 2017 during the X1.3 event. Note that the GNSS data from three more stations that are SLMA, PALM, and POAL were available. Data for INCO were unreliable and are not presented.

During the X1.3 event on day 07 the solar radio relative intensity reached smaller amplitudes compared to the X9.3 event on day 06 and similarly to the day 06 event the intensity at 1,436.49 MHz (close to L1) was less intense than for the L2C and L5. C/No fades and S4 fluctuations between 14:46–14.56 UT at the GPS L2C and L5 frequencies were observed simultaneously with increases in the radio flux relative intensity for all sites. Larger fades for L1 at 14:36 UT were observed for SLMA and PALM sites. The S4 peaks for L1, L2C and L5 were observed at all sites with larger S4 values for L1 (about 0.33) also for these two sites. POAL site, located

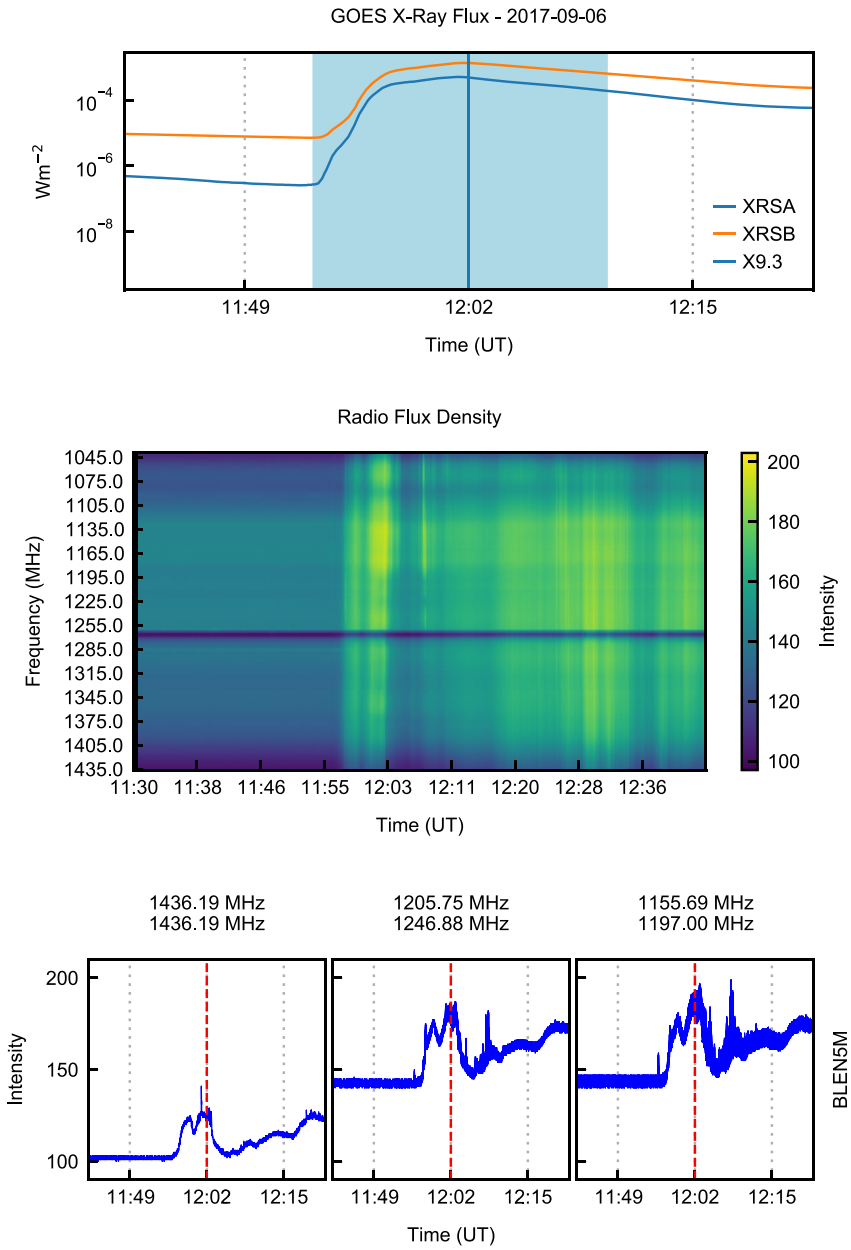

Figure 2. Solar X-ray flux (top), radio flux density from the frequency interval of 1,045–1,435 MHz (middle) and for three ranges of frequency during day 06 of September 2017.

beyond the EIA southern crest, presented the lowest values of C/No fades and S4 for L1 band and no fade and consequently no S4 amplitude fluctuations for L2C and L5.

4.2. Slant TEC Increases (SITEC) During the Events

Figure 8 presents the São José dos Campos (SJSP) (22.21°S, 45.85°W, dip latitude 19.59°S) slant TEC (STEC) for different PRNs from 11:00 to 13:00 UT for days 05–09 and the temporal resolution of the data used was 30 s. These data were provided by the RBMC/IBGE and can be downloaded directly from ftp://geoftp.ibge.gov.br/informacoes_sobre_posicionamento_geodesico/rbmc/. An elevation mask of 20° was adopted. The EUV 30.4 nm solar flux of day 06 from 11:50 to 12:30 UT is superimposed onto each GNSS satellite frame of Figure 8 (thin

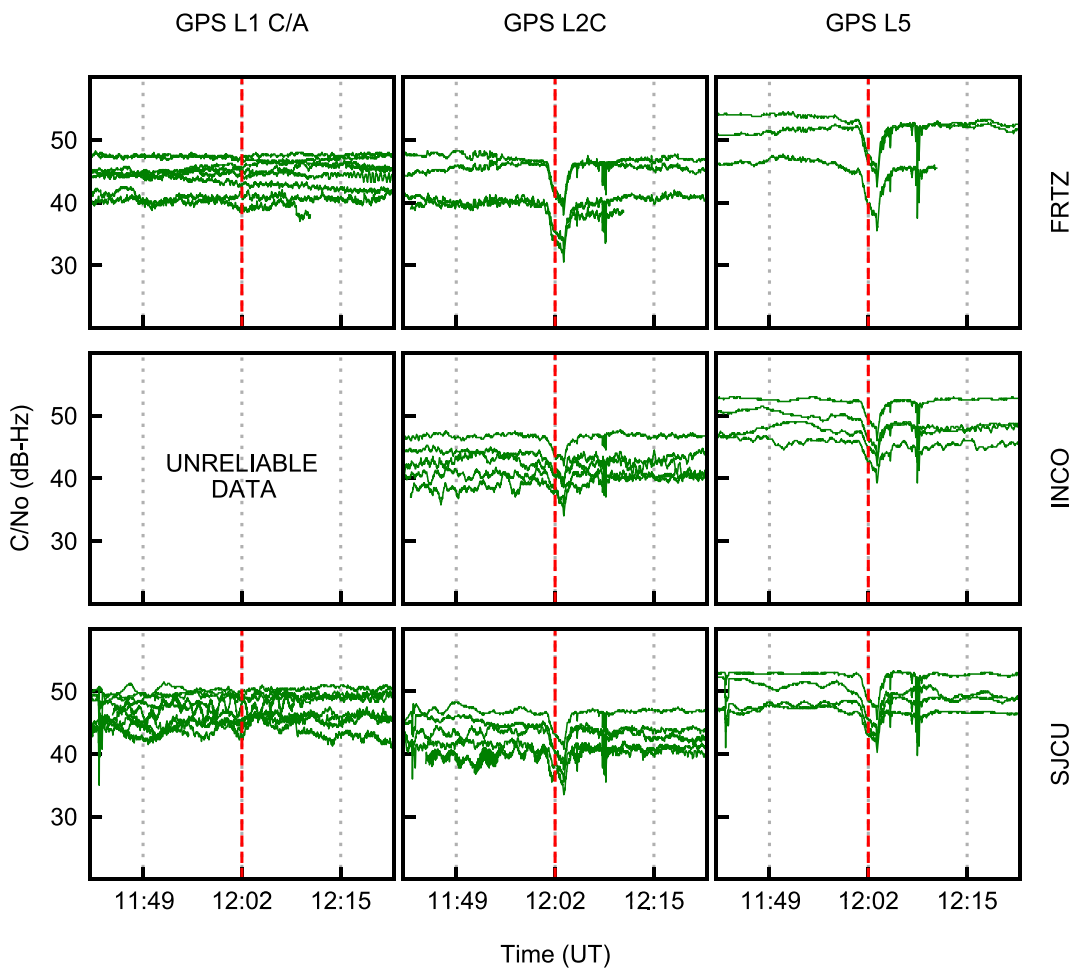

Figure 3. Global Positioning System (GPS) carrier-to-noise ratio signal for L1, L2C, and L5 GPS frequencies during day 06 for the sites FRTZ, INCO, and SJCU.

black lines). The EUV data were obtained from NASA Solar Dynamics Observatory data website http://lasp.colorado.edu/eve/data_access/evewebdata/products/.

Large sudden increases in TEC are observed for all satellites on day 06 during the X9.3 event, simultaneously with EUV increase. Each satellite measured different rates of sudden TEC increases on day 06 since their signals were crossing different regions of the ionosphere.

The EUV flux (thin black line on Figure 8) increase after around 11:55 UT caused simultaneous STEC increases at the low latitude SJSC station on day 06 (red line on Figure 8) of 2 TECU for PRN 22, 2.53 TECU for PRN 3, and 3.33 TECU for PRNs 1,7, 9, and 23. These TEC increases are comparable to the TEC increase of approximately 3 TECU for Neustrelitz, located at middle latitude, presented by Sato et al. (2019) for the PRN 27 (Figure 3 lower panel). The larger STEC increases at SJSP for PRNs 1,7, 9, and 23 compared to Neustrelitz (PRN 27) during this X9.3 solar flare are due to the proximity of SJSP to the EIA south crest and its lower latitude compared to Neustrelitz, however the satellite inclination and azimuth are also two factors to be considered. Shagimuratov et al. (2020) using GNSS data from mid-latitude stations found a linear relation between the ΔTEC, that is the amplitude of the TEC response to the flare from TEC measurements along the satellite passage, and the zenith angle of the sun for the X9.3 event on 06 September 2017. They observed ΔTEC increases for decreasing zenith angles. Their ΔTEC exceeded 3 TECU for the lowest zenith angle what is comparable with the SJSP maximum ΔTEC that was 3.3 TECU.

The temporal ROT was calculated using 30 s RBMC/IBGE data for SJSP from days 05–07 (see Figure 9 left panels). The day 05 was magnetically quiet. The corresponding ROTI index was calculated for each 5 min (see

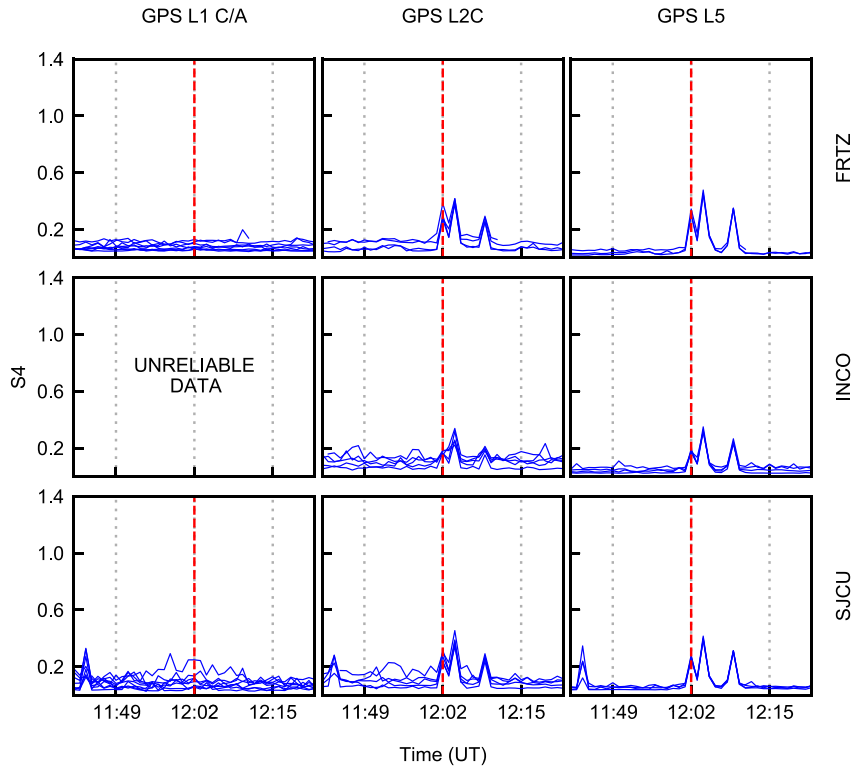

Figure 4. Signal amplitude fluctuations represented by the S4 parameter for all visible PRNs and for the sites FRTZ, INCO, and SJCU.

Figure 9 right panels). The methodology introduced by Pi et al. (1997) was used. Large ROT variations and ROTI values were observed during the X9.3 event on day 06 for all satellites. The results of ROT from left middle panel from the low latitude station of São José dos Campos agree quite well with the values found in Figure 8c of Y. Yasyukevich et al. (2018), even though such measurements were made in different longitudinal sector (Africa-Europe) using 10 near-equatorial and middle latitude GNSS receivers capturing the Beidou 05 geostationary satellite signals.

With the aim of studying the ROTI variation with latitude on day 06 the median value of this parameter was calculated using the available TEC data in the geographical longitudinal sector of 312.5 to 320°W (corresponding to 30 min) and in the geographical latitudes from 3 to 23°S with a latitudinal resolution of 1°. The results of this analysis are presented in Figure 10. Larger ROTI values during the X9.3 event time interval are observed in the region around the EIA southern crest.

4.3. Response to the Event as Recorded by Digisonde

Digisonde data are being used in the paper to show the effect of absorption of the HF signal because of the increase in ionization in the D region caused by X-rays. The f_{min} (minimum frequency registered by the Digisonde) parameter gives a good indication of this absorption. f_{min} rises sharply when absorption occurs and slowly decays after ascent. Figure 11 presents the f_{min} parameter for the sites of São Luís, Fortaleza, Campo Grande, and Cachoeira Paulista for days 06 and 07 September 2017. In this plot the dark gray and the light gray vertical bands represent respectively the time intervals of the occurrences of the X9.3 and X1.3 events. During these two events, gaps in the Digisonde signal can be observed due to signal absorption by increased D layer density caused by the short X-ray radiation intensification. The vertical red dashed lines represent the Storm Sudden Commencements on days 06 and 07.

The f_{min} parameter behavior for these four sites was very similar mainly after the X9.3 event, except for about 3 hr before the X9.3 and X1.3 events. Preceding the X9.3 event a short lived class X2.2 flare occurred starting at

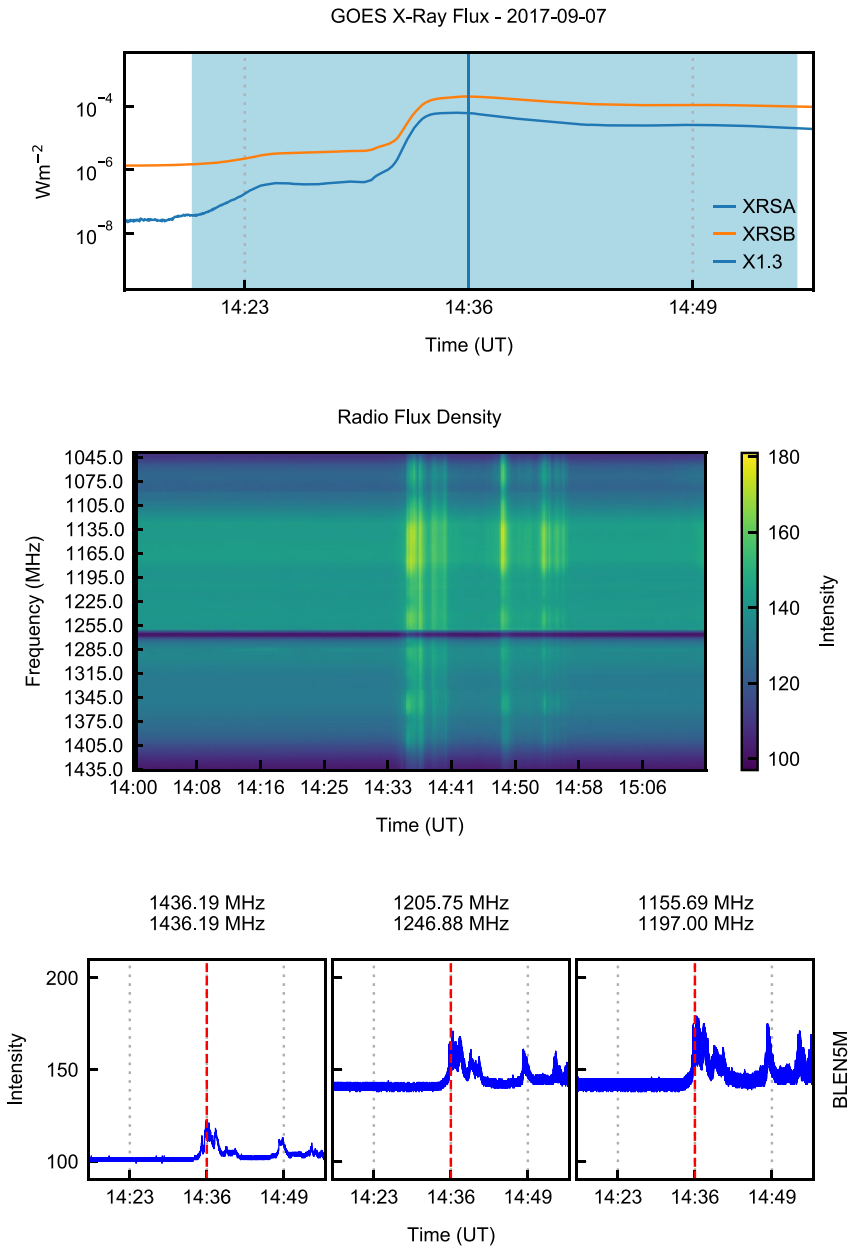

Figure 5. Solar X-ray flux (top), radio flux density from the frequency interval of 1,045–1,435 MHz (middle) and for the frequency of 1,436.19 MHz, for the frequency ranges 1,205.75–1,246.88 MHz and 1,155.69–1,197.00 MHZ (lower panel from left to right, respectively) for day 07 of September 2017.

08:57 UT with a maximum at 09:10 UT (Y. Yasyukevich et al., 2018) while before the X1.3 event a short lived class C2 event occurred. The f_{min} for Fortaleza and São Luís, located closer to the magnetic equator, presented much larger sudden increases than for Campo Grande and Cachoeira Paulista located at low latitudes, during the weaker events which occurred previously to the X9.3 and X1.3 events. On the other hand, during the strong events, like the X9.3, the f_{min} parameter, representing the HF signal absorption due to increased D layer electron density, tends to extend equally from equatorial to low latitudes sites.

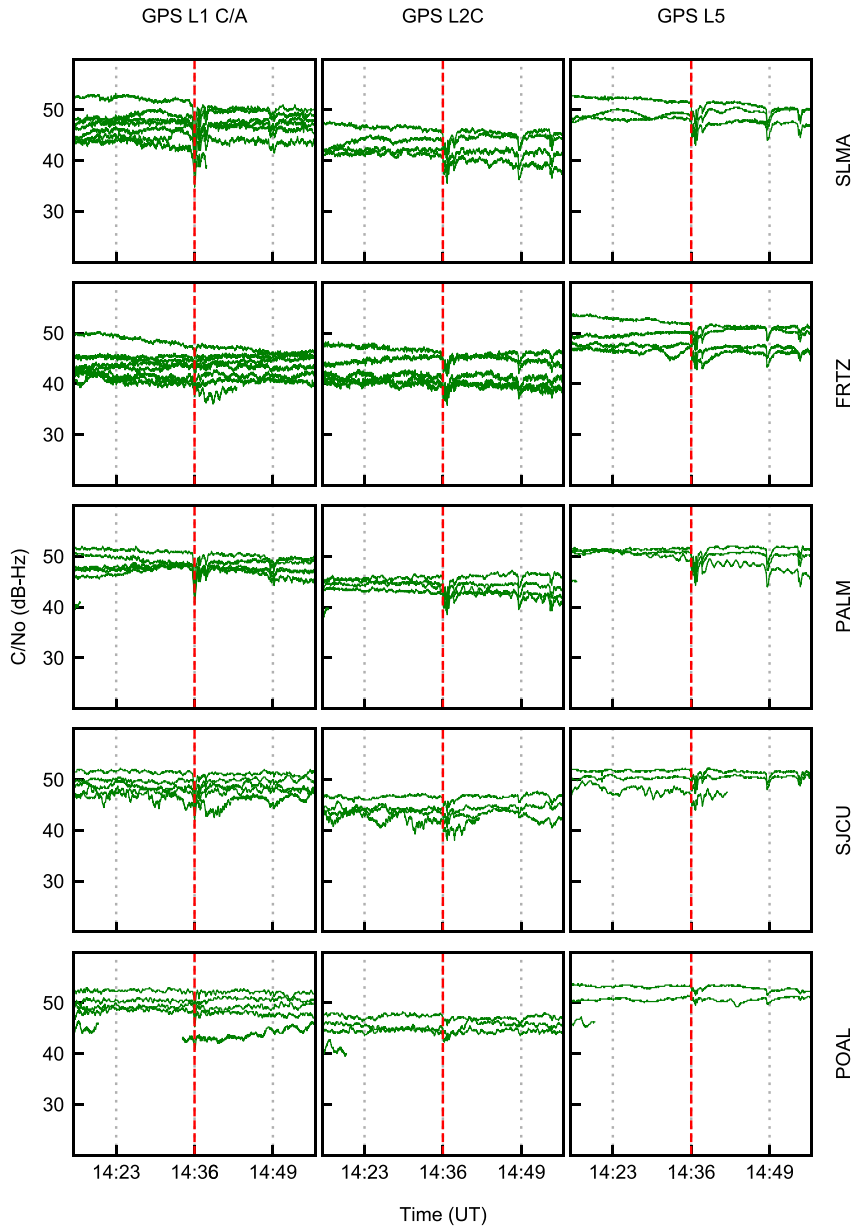

Figure 6. Global Positioning System (GPS) carrier-to-noise ratio signal for L1, L2C, and L5 GPS frequencies for day 07 and for the sites SLMA, FRTZ, PALM, SJCU, and POAL.

4.4. Equatorial and off Equatorial Magnetometer Data

Figure 12 presents the 1 minute magnetometer H component for the equatorial station Belém (01.12°S dip latitude) and for the off equatorial station Petrolina (13.45°S dip latitude). These data were provided by the AMBER magnetometer network at https://doi.org/10.5281/zenodo.6533221.

The events X9.3 and X1.3 time intervals are marked with red and orange vertical bands respectively. Short-lived increases in the H values were observed simultaneously with the events for Petrolina, while this parameter decreased during the X9.3 event and increased during the X1.3 event for Belém.

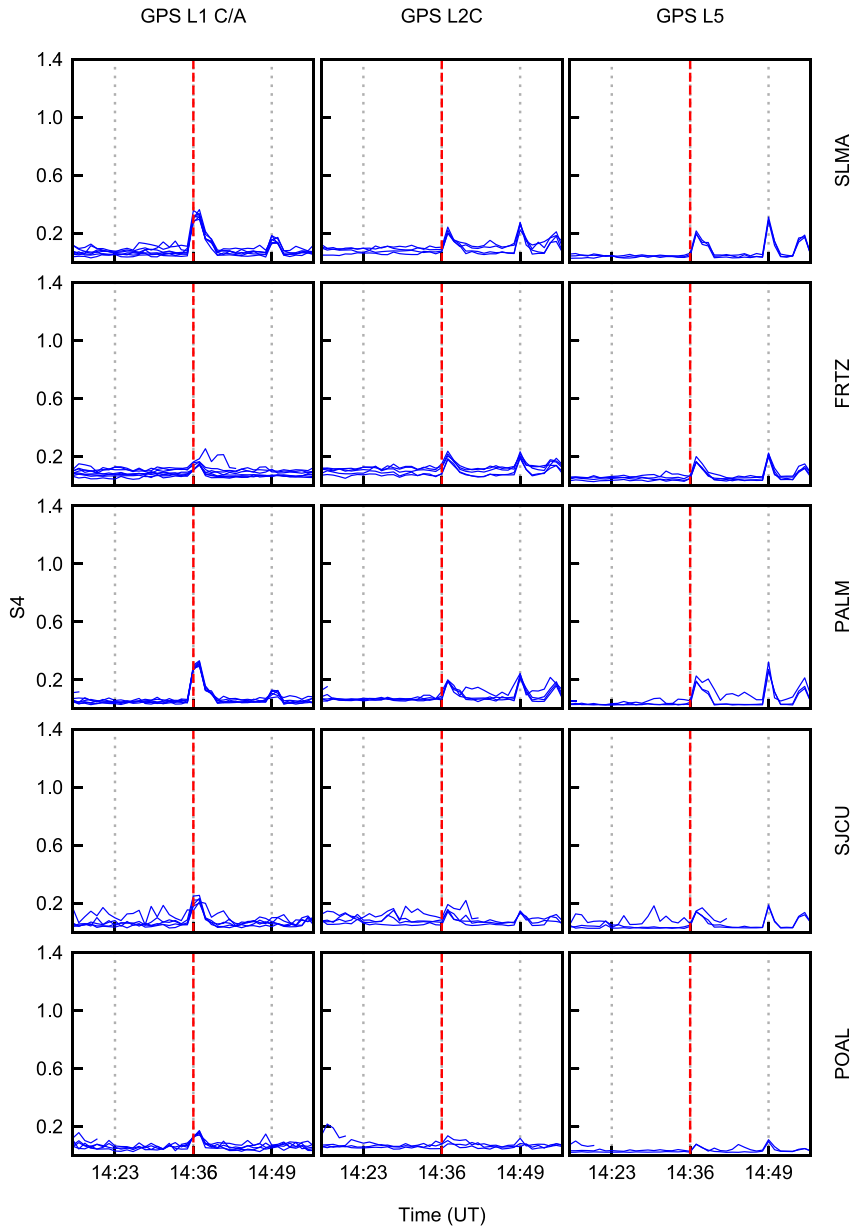

Figure 7. Signal amplitude fluctuations represented by the S4 parameter for all visible PRNs for day 07 for the sites SLMA, FRTZ, PALM, SJCU, and POAL.

4.5. Positioning Errors During the X9.3 and X1.3 Events Using RTKlib Software

The positioning errors analysis, using the RTKlib software (Takasu & Yasuda, 2009) for several GNS stations, including those from Figure 1 was carried out. As a representative GNSS station, we present results from SJSP during the X9.3 event on day 06 (day of the year: 249). The SJSP GNSS receiver belongs to RBMC/IBGE network and is located about 10 km apart from the receiver site SJCU. All other stations had similar behavior. For the positioning estimation the kinematic precise point positioning (PPP) was used with RTKPost and the following inputs: dual-frequency GPS data, precise ephemeris and antex files for antenna calibration from International GNSS Service, Differential Code Bias from Center for Orbit Determination in Europe for the correction of inter-frequency bias and Earth Orientation Parameters file from International Earth Rotation and Reference System Service to correct the irregularities of the Earth's rotation. In the processing, only data with an elevation angle larger than 10° was considered. The forward and the forward/backward processing approaches were used with the ITRF2014 adopted as a reference frame. The forward approach is normally used for real time application

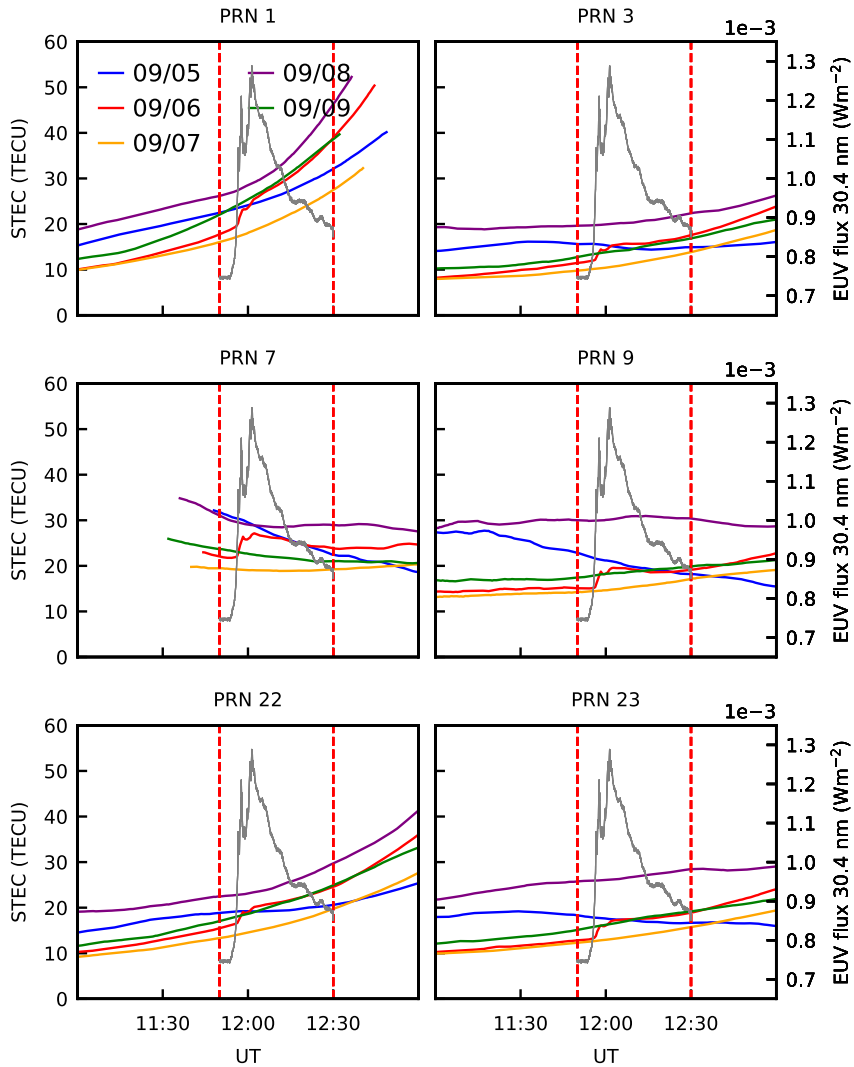

Figure 8. Slant Total Electron Content (STEC) for days 05–09 from different PRNs for São José dos Campos using Rede Brasileira de Monitoramento Contínuo/Instituto Brasileiro de Geografia e Estatística Global Positioning System data with a time resolution of 30 s. The vertical dashed lines mark the time interval 11:50–12:30 UT corresponding to the Enhanced UV solar flux (thin black line) for day 06 overlapped with STEC plots.

and the forward/backward for post processing. The ion-free observable was used to reduce the first order effects of the ionosphere. For the troposphere, the Zenithal Tropospheric Delay was estimated together with the gradients. The observed east (E), north (N), and vertical (U) positioning discrepancies relative to the known ITRF2014 positions and the estimated precision (sigma) during day 06 (249) September 2017 for SJSP are presented in Figure 13, considering the forward approach. Only the period from 10:00 to 15:00 UT is shown in order to highlight the X9.3 solar flare effects over the positioning. The other periods of time during day 06 did not show any anomaly. As for day 07 (250) there is no adverse occurrence in the results, they will not be presented. The sudden error increasing in the ENU components presented in Figure 13 is in accordance with the dual frequency PPP error results from Sato et al. (2019) in Neustrelitz, Germany. It is probably due to the occurrence of cycle slips as an effect of the solar flare X9.3. The algorithm restarts the ambiguities, requiring a new interval for convergence.

As stated before, the effect of the solar flare X9.3 on the positioning discrepancies and sigma at the other stations was similar to those at SJSP. For the forward approach, used for real time applications, the effects were quite more significant on several epochs during the event, reaching for example, about 0.67 m of discrepancy and 1.7 m sigma in the Up component. In the forward/backward approach, the effects were less pronounced, but just for one epoch (11:56:45 UTC) the discrepancies reach about 0.47 m in the N component and about 0.51 m sigma

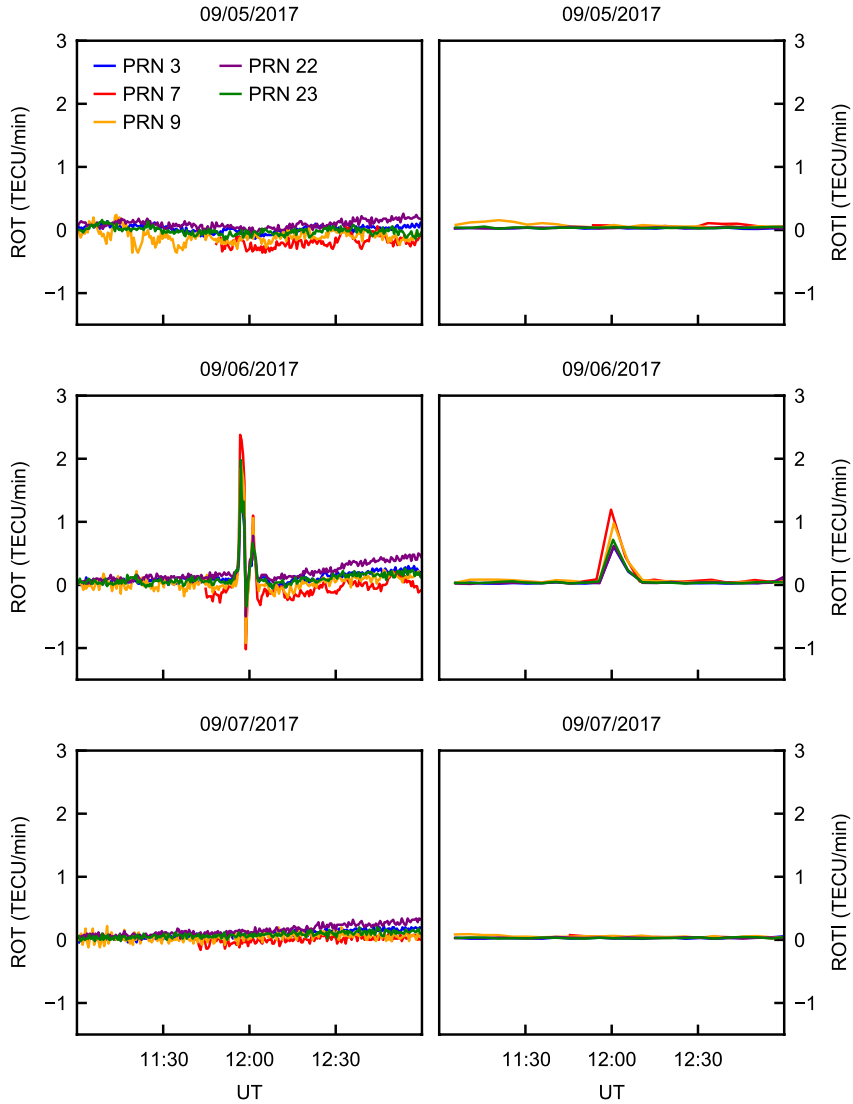

Figure 9. Rate of Total Electron Content (TEC) and Rate of TEC Index parameters for São José dos Campos during days 05, 06, and 07 for five PRNs.

in the Up component. If the data of the correspondent epoch is flagged as outlier and all data reprocessed again, the discrepancies will be eliminated. But it is only possible for post processing operations. As one can see from the results, the solar flare affected the positioning, mainly for the real time applications. Mitigation or warning for such occurrence is quite important for real time applications. For post processing, some improvement is possible to be obtained.

5. Discussions

This work presents the solar flare and radio burst effects on GNSS signals and the ionosphere during September 2017 using data from an array of GNSS receivers and Digisondes distributed from equatorial to low latitudes, and two magnetometers in the Brazilian longitudinal sector. Simultaneous Goes X-Ray flux, radio flux intensity and EUV solar flux are used to quantify their increases during the X9.3 and X1.3 events. Additionally positioning error analysis errors using the RTKlib software was performed. The analyses of the parameters C/No signal, TEC, ROT, ROTI, S4 (amplitude fluctuations), f_{min}, and magnetic H component inferred from these equipment during the X9.3 and X1.3 solar flares complement similar analyses made at different latitudinal and longitudinal sectors.

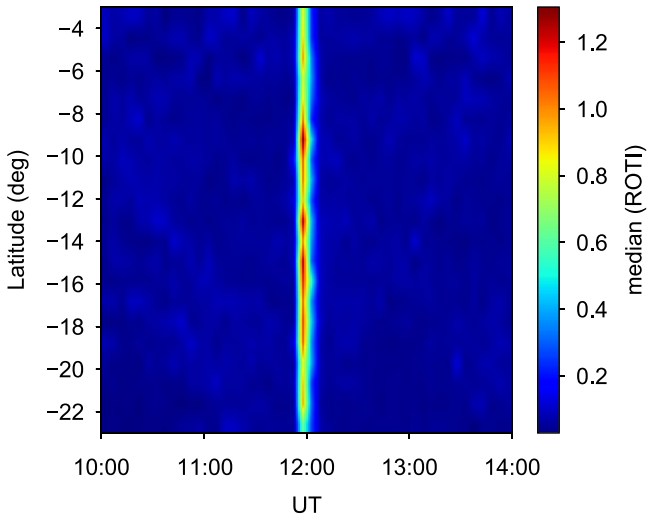

Figure 10. Median Rate of Total Electron Content (TEC) Index (ROTI) calculated in the longitudinal bin sector from 312.5 to 320°W and latitudinal resolution of 1° on day 06. The color bar presents the ROTI values in TECU/min.

During the solar flare events analyzed in this work simultaneous increases in the X-ray and EUV fluxes and SRBs were observed. SRBs can affect the GNSS signals while X-ray and EUV increases produce sudden ionization in the ionospheric layers. Carrano et al. (2009) pointed out that the solar incidence angle affects C/No fades during the SRBs, however our work did not account for this effect since the sites are not far from each other. Similar C/No fades were detected for the GLONASS and Galileo constellations and for the SBAS signals simultaneously with the events (not shown at this work). C/No fades and signal fluctuations represented by the S4 indices during the two events presented latitudinal variations, being larger for sites closer to the equator. The ROTI during the X9.3 event was larger for regions around the EIA crest, which to some extent is expected because this parameter is proportional to the TEC.

During the X9.3 event C/No fades varying from 5 to 10 dB and S4 values reaching about 0.40 were observed around 12:02 UT for the L2C and L5 on day 06. Their amplitudes were larger for the FRTZ site closer to the equator, decreased for SJCU under the EIA and the lowest values were for the INCO site. Secondary peaks of these two parameters with lower amplitudes occurred around 12:08 UT simultaneously with solar relative intensity increase. No C/No fades and S4 increases were observed in the L1 frequency. The relative solar intensity in the L1 frequency was lower than for the L2C and L5 frequencies during this event.

During the X1.3 event C/No fades of about 5 dB and S4 values of about 0.2–0.33 (this higher value is for PALM and SLMA) were observed simultaneously with the solar flare relative intensity increases at about 14:36, 14:48, and 14:55 UT for L2C and L5. Their amplitudes increased from high to low latitude with stations FRTZ and PALM presenting similar amplitudes. For the L1 frequency, fades in the C/No of about 5 dB were observed for SLMA and PALM. S4 values increased for lower latitudes, being the higher S4 value of about 0.33 at SLMA and PALM.

Comparing the C/No fades and S4 values for the two events, their amplitudes at the GPS frequencies L2C and L5 were larger for the X9.3 event. So the SRB intensity level is a determining factor for the signal C/No fades and amplitude fluctuation severity. During the maximum intensity of the X9.3 event on day 06 at about the morning hour 09:02 LT (LT = UT − 3), the ionospheric electron density was about 1×10^6 electrons/cm^3, while during the event X1.3 at about 11:46 LT (noon hour) this density was 1.2×10^6 electrons/cm^3, that is 20% larger.

Sudden increases in the TEC rates of 2.5–5.0 TECU/min for the X9.3 event were observed at different PRNs with 10–12 min of duration for all sites and for all satellites. The X-rays fluxes were one order of magnitude larger for the X9.3 event compared to the X1.3 event.

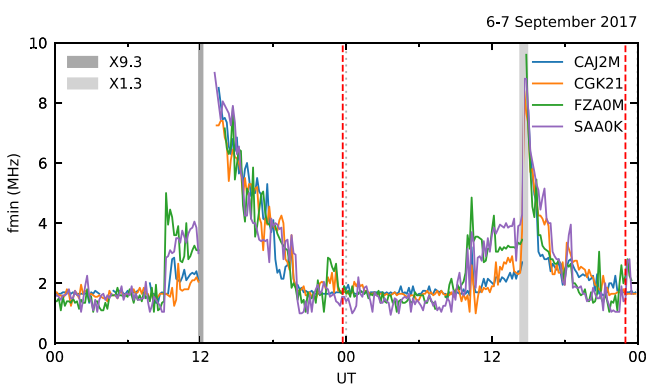

Figure 11. f_{min} Digisonde parameter for São Luís (SAA0K), Fortaleza (FZA0M), Campo Grande (CGK21), and Cachoeira Paulista (CAJ2M).

Gaps in the ionogram f_{min} parameter inferred from four Digisonde sites shown as blue stars at Figure 1, were noticed during the events (see Figure 11). These ionogram gaps were due to the total or partial absorption of the HF wave by the increased D region density due to the intensified short X-ray radiation characterizing the flares. About 3 hours anteceding the two events X9.1 and X1.3 sharp f_{min} increases were observed, being the large ones for São Luís and for Fortaleza that are closer to the magnetic equator. These increases are related to other two weaker X-ray flares. These f_{min} increases remain up to the events when gaps were observed followed by very high f_{min} values. No signal gaps were observed at the site of São Luís for the X1.3 event.

Short lived fluctuations in the H component were observed (see Figure 12) simultaneously with the maximum intensity of the two events. The probable cause of these H variations is the solar flare induced increase in the ionospheric E layer densities enhancing the conductivities of this layer and consequently the ionospheric electric currents (Equatorial Electrojet (EEJ))

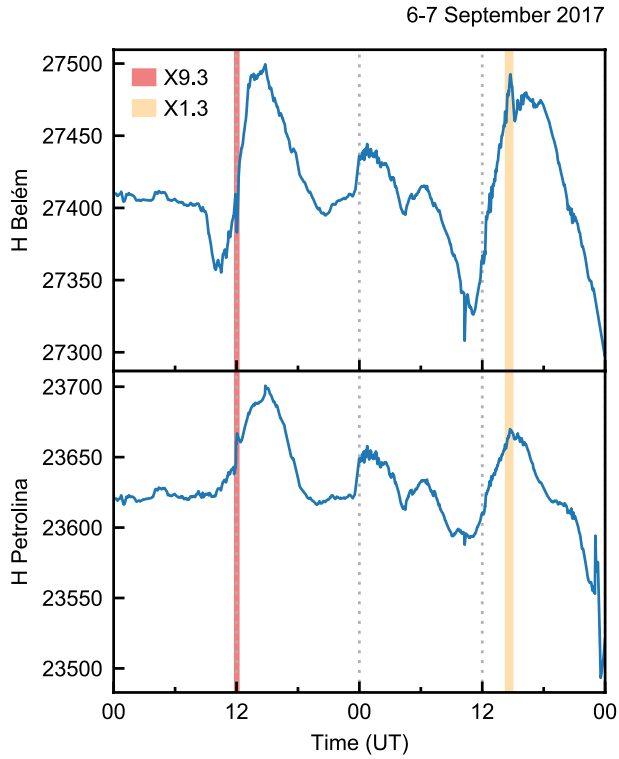

Figure 12. Belém (equatorial station) and Petrolina (off equatorial station) magnetometer horizontal component H.

that depending of the direction can reinforce or weaken the H component According to Abdu et al. (2017) "the flare-induced EEJ enhancement is proportional to, and in the same sense as, the immediately preexisting EEJ current." Simultaneous decrease of H component at Belém and increase at Petrolina for the event X9.3 and increase for both sites during the event X1.3 were observed. These different response features are due to the different local times at the two stations. In the first case (X9.3) the event occurred close to the morning hours (09:00 LT), probably still under the influence of a counter-electrojet recovery phase, while in the second case the flare effect occurred near midday (11:36 LT) when the eastward EEJ was well established (Abdu et al., 2017). Abdu et al. (2017) discuss nicely the complexity of the solar flare effects over the EEJ when it occurs simultaneously with the penetration to low latitudes of the Disturbance Dynamo Electric Field (DDEF) (westward during daylight hours) and during the Prompt Penetration Electric Field (PPEF) penetration (westward or eastward during daylight hours). According to Figure 1 of de Paula et al. (2019) Sym-H and interplanetary eastward electric field E_y values were 0 nT and 0 mV/n respectively during the X9.1 on day 06. During the X1.3 solar flare on day 07 the Sym-H was also 0 nT and E_y was westward but with a very low value of −4 mV/m. So no substantial magnetic storm effects were underway during the X9.1 and X1.3 events.

The positioning errors analysis during the X9.3 and X1.3 events, using the RTKlib software was carried out for SJSP. In the positioning estimation the kinematic PPP using RTKPost with the forward (for real time processing) and forward/backward (for post processing) approaches were used. In the forward approach, positioning discrepancies and large sigmas were observed at all sites only during the X9.3 event, which agrees with other results presented in the literature by Y. Yasyukevich et al. (2018), Berdermann et al. (2018), and Monico et al. (2019). For the forward approach, the flare effects were more significant than in the forward/backward approach, wherein the effects were reduced. So for real time applications, mitigation or warning during large solar flares are important procedures to be performed. A decrease was observed in the available GNSS satellites used in the positioning computations after the X9.3 maximum at 12:02 UT.

Similar to our work, Sato et al. (2019) observed significant deviations from the reference coordinates in the east, north, and height components using dual-frequency and single-frequency PPP at Neustrelitz on 06 September 2017 during the X9.3 event. Large sudden increases in TEC, due to the EUV flux intensification, were observed in both Germany and Brazilian longitudinal sectors. One interesting result is that during the X9.3 event, larger C/No fades on the frequencies L2C and L5 for receivers closer to the equator were observed in agreement with Sato et al. (2019) where C/No fades were also larger for the lower latitude site of Bahir Dar. GNSS receivers located close to the subsolar point (occurring at the geographic equator in September) tend to experience larger C/No fades because the intensity of solar radio noise is the largest at normal incidence. Also, the gain of a GNSS antenna is largest in the zenith direction, so the solar radio noise at the zenith is amplified more than signals from satellites that are not at the zenith. All of our stations are relatively close together geographically and the differences in solar incidence angles at these stations are relatively small, compared to those in the Sato el al. (2019) study. In addition to these similar topics considered in our work and Sato's in different longitudinal sectors, we pointed out the flare effects on the Digisonde parameter f_{min} and on the magnetic H component and we suggested the physical mechanisms responsible for them.

So, depending of the solar burst intensity and the frequency range of the radio flux density the GNSS receiver signal-to-noise ratio (C/No) can be faded due to the elevated background noise during the events. These fades can cause inaccurate navigation solution that could affect the positioning and navigation systems.

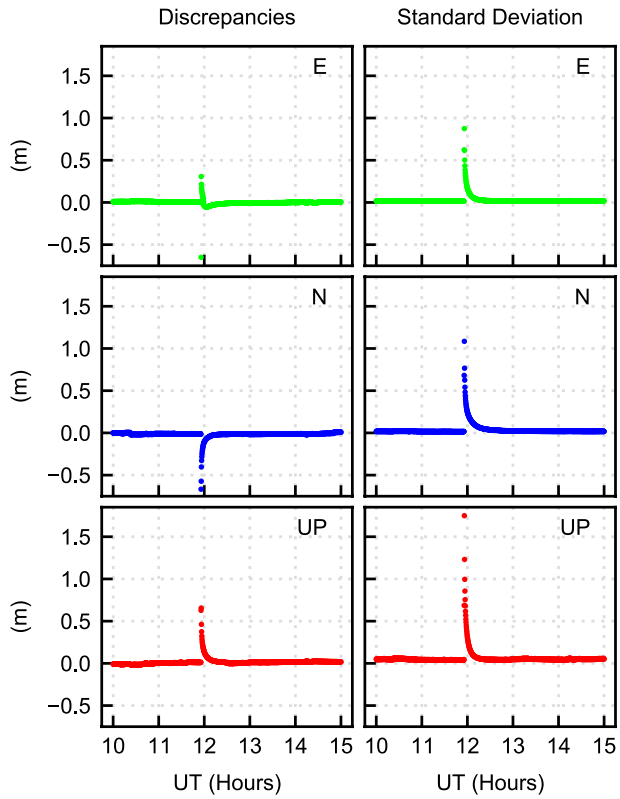

Figure 13. Observed east (E), north (N), and vertical (U) positioning discrepancies relative to the known ITRF2014 positions and the precision sigma for São José dos Campos station data during the day 06 (day of the year 249) considering the forward approach.

6. Conclusions

The main conclusions of this work are:

- The GNSS C/No signal fades decrease with increasing latitude and with decreasing solar flare intensity (see Figures 3 and 6).
- Similar behavior as in the previous statement is observed for the signal amplitude scintillations represented by the S4 index (see Figures 4 and 7).
- Variations are observed in the sudden STEC increases on day 06 (event X9.3) for different satellites with different inclinations since their line-of-sight paths cross different ionospheric regions (see Figure 8).
- ROT parameter presents short lived amplitude variations only for day 06 (X9.3) (see Figure 9).
- Clear median ROTI increases close to the southern Equatorial Ionization Anomaly crest were observed (see Figure 10).
- The Digisonde f_{min} parameter, representing the HF signal absorption due to increased D layer electron density, for four sites located at equatorial (close) to low latitudes, showed a larger increase for the stations of São Luís and Fortaleza that are closer to the magnetic equator. These increases were observed during two solar flare events with less intensity that occurred about 3 hr of antecedence from the events X9.3 and X1.3. After the large event X9.3 the f_{min} parameter behavior was similar at the four Digisonde sites with different latitudes and longitudes. Gaps in the time history of observed f_{min} values occur during the peaks of the X9.3 and X3.1 events due to very high absorption throughout the range of swept frequencies (see Figure 11).
- The behavior of the magnetometer H component during a flare event is highly dependent of the preexisting EEJ current. The magnetic storm PPEF or DDEF (or both sometimes) conditions, if existing, should be accounted for during the flare event. In this work we showed that on day 06 and 07 during the X9.3 and X3.1 events respectively, no magnetic storm effects were present (see Figure 12).
- The positioning errors analysis, using the RTKlib software, demonstrated that errors were observed only for the larger event X9.3 (see Figure 13).

This work may contribute to a better understanding of the ionospheric physics involved in solar flares and how to mitigate their effects on the GNSS positioning and navigation systems.

Similar analyses will be performed in similar studies on more solar flare events to test methods of mitigation, like the one used by Vani et al. (2019), to reduce the positioning deterioration during strong flare events.

Data Availability Statement

X class solar flares characteristics on 06 and 07 September 2017 were obtained from ftp.swpc.noaa.gov/pub/warehouse/2017/2017_events.tar.gz. GOES X-Ray flux data were acquired from https://satdat.ngdc.noaa.gov/sem/goes/data/science/xrs/goes15/gxrs-l2-irrad_science/2017/09/. Callisto spectrograms, for SWISS-BLEN5M observatory, were obtained from http://soleil.i4ds.ch/solarradio/data/2002-20yy_Callisto/2017/09/06/. CIGALA/CALIBRA GNSS RINEX and ISMR data were obtained from ISMR Query Tool website. First, is necessary to register an account at https://ismrquerytool.fct.unesp.br/is/ismrtool/registration/index.php?lan=en. After registration, proceed with login at https://ismrquerytool.fct.unesp.br/is/login/login.php?lan=en. In order to obtain the CIGALA/CALIBRA data go to menu ISMR Query Tool, in the top of the page, and access "Download ISMR" or "Download RINEX." IBGE RMBC GNSS RINEX data were obtained from http://geoftp.ibge.gov.br/informacoes_sobre_posicionamento_geodesico/rbmc/dados/. EUV flux 30.4 nm data were obtained from http://lasp.colorado.edu/eve/data_access/evewebdata/products. Belém and Petrolina Magnetometer data were obtained from

AMBER magnetometer data center and made available at https://doi.org/10.5281/zenodo.6533221. The digisonde data were obtained from http://www2.inpe.br/climaespacial/portal/ionosondes-home/, under registration.

Acknowledgments
E. R. de Paula is thankful for the support of CNPq through Grant 302531/2019-0. A. R. F. Martinon would like to acknowledge the support from FAPESP Grant 2018/23754-4. J. F. G. Monico and E. R. de Paula would like to acknowledge the INCT GNSS-NavAer Grants 2014/465648/2014-2 CNPq and 2017/50115-0FAPESP. INPE's authors thank the Brazilian Ministry of Science, Technology and Innovation and the Brazilian Space Agency.

References

Abdu, M. A., Nogueira, P. A. B., Souza, J. R., Batista, I. S., Dutra, S. L. G., & Sobral, J. H. A. (2017). Equatorial electrojet responses to intense solar flares under geomagnetic disturbance time electric fields. *Journal of Geophysical Research: Space Physics*, *122*(3), 3570–3585. https://doi.org/10.1002/2016JA023667

Berdermann, J., Kriegel, M., Banys, D., Heymann, F., Hoque, M. M., Wilken, V., et al. (2018). Ionospheric response to the X9.3 flare on 6 September 2017 and its implication for navigation services over Europe. *Space Weather*, *16*(10), 1604–1615. https://doi.org/10.1029/2018SW001933

Carrano, C. S., Bridgwood, C. T., & Groves, K. M. (2009). Impacts of the December 2006 solar radio bursts on the performance of GPS. *Radio Science*, *44*(1), RS0A25. https://doi.org/10.1029/2008RS004071

Cerruti, A. P., Kintner, P. M., Gary, D. E., Lanzerotti, L. J., de Paula, E. R., & Vo, H. B. (2006). Observed solar radio burst effects on GPS/Wide Area Augmentation System carrier-to-noise ratio. *Space Weather*, *4*(10), S10006. https://doi.org/10.1029/2006SW000254

Cerruti, A. P., Kintner, P. M., Jr., Gary, D. E., Mannucci, A. J., Meyer, R. F., Doherty, P., & Coster, A. J. (2008). Effect of intense December 2006 solar radio bursts on GPS receivers. *Space Weather*, *6*(10), S10D07. https://doi.org/10.1029/2007SW000375

Curto, J. J., Marsal, S., Blanch, E., & Altadill, D. (2018). Analysis of the solar flare effects of 6 September 2017 in the ionosphere and in the Earth's magnetic field using spherical elementary current systems. *Space Weather*, *16*(11), 1709–1720. https://doi.org/10.1029/2018SW001927

de Paula, E. R., Martinon, A. R. F., Moraes, A. O., Carrano, C., Neto, A. C., Doherty, P., et al. (2021). Performance of 6 different global navigation satellite system receivers at low latitude under moderate and strong scintillation. *Earth and Space Science*, *8*(2), e2020EA001314. https://doi.org/10.1029/2020EA001314

de Paula, E. R., Oliveira, C. B. A., Caton, R. G., Negreti, P. M. S., Batista, I. S., Martinon, A. R. F., et al. (2019). Ionospheric irregularity behavior during the September 6–10, 2017 magnetic storm over Brazilian equatorial-low latitudes. *Earth Planets and Space*, *71*(42), 42. https://doi.org/10.1186/s40623-019-1020-z

Hajra, R., Tsurutani, B. T., & Lakhina, G. S. (2020). The complex space weather events of 2017 September. *The Astrophysical Journal*, *899*(1), 3. https://doi.org/10.3847/1538-4357/aba2c5

Klobuchar, J. A., Kunches, J. M., & Van Dierendonck, A. J. (1999). Eye on the ionosphere: Potential solar radio burst effects on GPS signal to noise. *GPS Solutions*, *3*(2), 69–71. https://doi.org/10.1007/PL00012794

Liu, J.-Y., Lin, C. H., Chen, Y. I., Lin, Y. C., Fang, T. W., Chen, C. H., et al. (2006). Solar flare signatures of the ionospheric GPS total electron content. *Journal of Geophysical Research*, *111*(A5), A05308. https://doi.org/10.1029/2005JA011306

Mitra, A. P. (1974). *Ionospheric effects of solar flares* (p. 294). Springer. https://doi.org/10.1007/978-94-010-2231-6

Monico, J. F., Silva, W. C., de Paula, E. R., & Martinon, A. R. F. (2019). PPP effects due to the September 6 to 10, 2017 magnetic storm over Brazilian low latitudes. (2019). In *Paper presented at 7th international colloquium on scientific and fundamental aspects of GNSS*. 4-6 September 2019.

Nogueira, P. A. B., Souza, J. R., Abdu, M. A., Paes, R. R., Sousasantos, J., Marques, M. S., et al. (2015). Modeling the equatorial and low-latitude ionospheric response to an intense X-class solar flare. *Journal of Geophysical Research: Space Physics*, *120*(4), 3021–3032. https://doi.org/10.1002/2014JA020823

Pi, X., Mannucci, A. J., Lindqwister, U. J., & Ho, C. M. (1997). Monitoring of global ionospheric irregularities using the worldwide GPS network. *Geophysical Research Letters*, *24*(18), 2283–2286. https://doi.org/10.1029/97gl02273

Sato, H., Jakowski, N., Berdermann, J., Jiricka, K., Heßelbarth, A., Banyś, D., & Wilken, V. (2019). Solar radio burst events on 6 September 2017 and its impact on GNSS signal frequencies. *Space Weather*, *17*, 816–826. https://doi.org/10.1029/2019SW002198

Shagimuratov, I. I., Zakharenkova, I. E., Tepenitsina, N. Y., Yakimova, G. A., & Efishov, I. I. (2020). Ionospheric effects of solar flares in September 2017 and an evaluation of their influence on errors in navigation measurements. *Geomagnetism and Aeronomy*, *60*(5), 597–605. https://doi.org/10.1134/s0016793220050138

Sreeja, V., Aquino, M., & de Jong, K. (2013). Impact of the 24 September 2011 solar radio burst on the performance of GNSS receivers. *Space Weather*, *11*(5), 306–312. https://doi.org/10.1002/swe.20057

Sripathi, S., Balachandran, N., Veenadhari, B., Singh, R., & Emperumal, K. (2013). Response of the equatorial and low-latitude ionosphere to an intense X-class solar flare (X7/2B) as observed on 09 August 201. *Journal of Geophysical Research: Space Physics*, *118*(5), 2648–2659. https://doi.org/10.1002/jgra.50267

Takasu, T., & Yasuda, A. (2009). Development of the low-cost RTK-GPS receiver with an open source program package RTKLIB. In *Paper presented at International Symposium on GPS/GNSS* (p. 6). International Convention Center. Retrieved from http://gpspp.sakura.ne.jp/paper2005/isgps_2009_rtklib_revA.pdf

Tsurutani, B. T., Verkhoglyadova, O. P., Mannucci, A. J., Lakhina, G. S., Li, G., & Zank, G. P. (2009). A brief review of "solar flare effects" on the ionosphere. *Radio Science*, *44*(01), 1–14. https://doi.org/10.1029/2008RS004029

Vani, B. C., Forte, B., Monico, J. F. G., Skone, S., Shimabukuro, M. H., de Oliveira Moraes, A., et al. (2019). A novel approach to improve GNSS precise point positioning during strong ionospheric scintillation: Theory and demonstration. *IEEE Transactions on Vehicular Technology*, *68*(5), 4391–4403. https://doi.org/10.1109/tvt.2019.2903988

Yasyukevich, Y., Astafyeva, E., Padokhin, A., Ivanova, V., Syrovatskii, S., & Podlesnyi, A. (2018). The 6 September 2017 X-class solar flares and their impacts on the ionosphere, GNSS, and HF radio wave propagation. *Space Weather*, *16*(8), 1013–1027. https://doi.org/10.1029/2018SW001932

Yasyukevich, Y. V., Yasyukevich, A. S., & Astafyeva, E. I. (2021). How modernized and strengthened GPS signals enhance the system performance during solar radio bursts. *GPS Solutions*, *25*(2), 46. https://doi.org/10.1007/s10291-021-01091-5

Yue, X., Wan, W., Yan, L., Sun, W., Hu, L., & Schreiner, W. S. (2018). The effect of solar radio bursts on GNSS signal. In *Chapter 22, extreme events in geospace*. Elsevier. https://doi.org/10.1016/B978-0-12-812700-1.00022-4